Ni2+-binding RNA motifs with an asymmetric purine-rich internal loop and a G-A base pair

H. P. Hofmann, S. Limmer, V. Hornung and M. Sprinzl

RNA 1997 3: 1289-1300

RNA (1997), *3*:1289–1300. Cambridge University Press. Printed in the USA.

Ni^{2+}-binding RNA motifs with an asymmetric purine-rich internal loop and a G-A base pair

HANS-PETER HOFMANN, STEFAN LIMMER, VERONIKA HORNUNG, and MATHIAS SPRINZL

Laboratorium für Biochemie, Universität Bayreuth, D-95440 Bayreuth, Germany

ABSTRACT

RNA molecules with high affinity for immobilized Ni^{2+} were isolated from an RNA pool with 50 randomized positions by in vitro selection-amplification. The selected RNAs preferentially bind Ni^{2+} and Co^{2+} over other cations from first series transition metals. Conserved structure motifs, comprising about 15 nt, were identified that are likely to represent the Ni^{2+} binding sites. Two conserved motifs contain an asymmetric purine-rich internal loop and probably a mismatch G-A base pair. The structure of one of these motifs was studied with proton NMR spectroscopy and formation of the G-A pair at the junction of helix and internal loop was demonstrated. Using Ni^{2+} as a paramagnetic probe, a divalent metal ion binding site near this G-A base pair was identified. Ni^{2+} ions bound to this motif exert a specific stabilization effect. We propose that small asymmetric purine-rich loops that contain a G-A interaction may represent a divalent metal ion binding site in RNA.

Keywords: in vitro selection; metal ion binding; NMR; mismatch base pairs

INTRODUCTION

Most RNA molecules require the presence of divalent metal ions to gain physiological activity. Two effects are assumed to be especially important. Structurally acting divalent metal ions bind to RNA and are indispensable for the formation of the proper tertiary structure. Furthermore, catalytic activity of RNA enzymes (ribozymes) depends on the presence of divalent metal ions, which are thought to be involved directly in the catalytic mechanism (Pan et al., 1993; Pyle, 1993; Yarus, 1993).

Several techniques have been applied to localize metal ion binding sites on RNA and to determine the precise binding geometry. X-ray crystallographic studies of yeast $tRNA^{Phe}$ (Jack et al., 1977), the hammerhead ribozyme (Pley et al., 1994; Scott et al., 1995, 1996), and a domain of the *Tetrahymena* group I intron (Cate et al., 1996) revealed principles of RNA tertiary structure stabilization by divalent metals ions and led to models for the catalytic role of metal ions. The broadening of NMR resonances upon adding paramagnetic Mn^{2+} or Co^{2+} was analyzed to localize metal ion binding sites on tRNA (Hurd et al., 1979). The same method was used recently to study metal ion binding to short RNA duplexes by high-resolution NMR (Ott et al., 1993; Allain & Varani, 1995). Phosphate groups involved in coordination of Mg^{2+} ions can be identified with the technique of "manganese rescue" (Christian & Yarus, 1993). In these experiments, loss of RNA activity upon substitution of sulfur for phosphate oxygens is reduced by adding Mn^{2+}, which has a higher affinity for sulfur compared to Mg^{2+}. Metal-induced cleavage of phosphodiester bonds can be used to roughly localize metal ion binding sites (Brown et al., 1983; Kazakov & Altman, 1991; Ciesiolka et al., 1995).

Isolation of functional RNA molecules from random pools by repeated cycles of in vitro selection and amplification (Ellington & Szostak, 1990; Tuerk & Gold, 1990) is a technique for a wide range of applications. These include the study of RNA–protein interaction (Bartel et al., 1991), the selection of RNA molecules that bind to small ligands with high affinity and specificity (Jenison et al., 1994), the search for ribozymes with new catalytic activities (Lorsch & Szostak, 1996), and the isolation of RNAs as potential diagnostic and therapeutic agents (Uphoff et al., 1996). In vitro selection techniques have also been applied to study the interaction of metal ions and RNA. The activity of the *Tetrahymena* group I intron is strictly Mg^{2+}- or Mn^{2+}-dependent (Grosshans & Cech, 1989). Lehman and Joyce (1993) used the in vitro selection method to isolate variants of the ribozyme that could function in the

Reprint requests to: Mathias Sprinzl, Laboratorium für Biochemie, Universität Bayreuth, D-95440 Bayreuth, Germany; e-mail: mathias.sprinzl@uni-bayreuth.de.

presence Ca^{2+}. Pb^{2+}-dependent ribozymes were selected by Pan and Uhlenbeck (1992a, 1992b) as an extension of the well-known Pb^{2+}-induced self-cleavage of yeast $tRNA^{Phe}$ (Brown et al., 1983). The tRNA analogue was randomized at several positions, and molecules that retained Pb^{2+}-dependent self-cleavage activity were isolated. Surprisingly, most of the selected variants had altered cleavage positions, indicating different Pb^{2+} binding sites. More recently, an RNA that binds Zn^{2+} was selected from a pool with 50 randomized positions (Ciesiolka et al., 1995). The metal ion binding site was localized at the junction of a long helix and a large hairpin loop. Randomization of the loop region and reselection of this pool led to isolation of several families of Zn^{2+}-binding RNA motifs (Ciesiolka & Yarus, 1996).

We have selected RNA molecules that bind Ni^{2+}, a transition metal that is a catalytically active component in several protein enzymes (Hausinger, 1993). This metal ion has not yet been identified in connection with RNA function. As we show here, RNA can form structures with high affinity and specificity for Ni^{2+} ions. Furthermore, it is demonstrated that Ni^{2+} is well suited as a paramagnetic probe to study metal ion–RNA interaction by NMR. Polymer matrix that contains Ni^{2+}-nitrilo-tri-acetic acid (NTA) complexes is widely used to immobilize His-tagged proteins. Such immobilized proteins can be potentially used for the isolation of protein-binding RNA aptamers. For this approach, it is useful to know the structure of RNA aptamers with affinity for immobilized Ni^{2+}, which may be obtained when the Ni^{2+}-NTA material is not completely saturated with the His-tagged protein.

RESULTS

Selection and sequences of Ni^{2+}-binding RNAs

Ni^{2+} ions are immobilized on Ni-NTA resin through the NTA unit, which occupies four of the six ligand binding sites in the coordination sphere of Ni^{2+} (Fig. 1). The two remaining coordination sites are accessible for interaction with another ligand. This resin

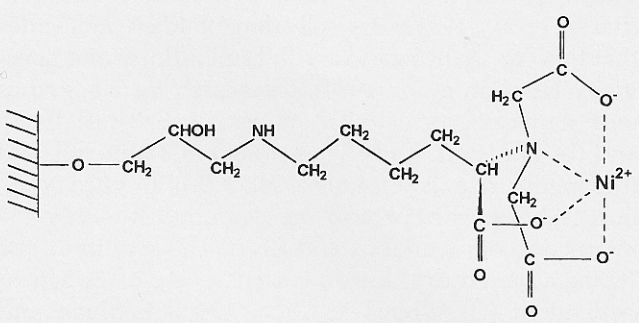

FIGURE 1. Structure of Ni-NTA resin used for in vitro selection of Ni^{2+}-binding RNA molecules.

is commonly used to purify proteins with an extension of histidines at either the N-terminus or C-terminus (His tag). The proteins bind to the matrix by coordination of two imidazole nitrogens to the Ni^{2+} ion, and elution is achieved by competition with excess imidazole. The same strategy was used to isolate RNAs that interact with the Ni-NTA matrix from an RNA pool with a randomized region of 50 nt. In the first five cycles of selection and amplification, 0.2–0.8% of total RNA remained bound to the matrix. A strong increase in binding was observed up to the sixth round and, after eight cycles, 27% of the total RNA remained bound to the Ni-NTA resin.

The PCR product corresponding to the selected RNA of the last cycle was cloned. Twenty-eight individual clones were sequenced, which led to 13 different sequences (Fig. 2). Clones N1, N9, and N11 were the most abundant ones. The selected RNA molecules contain significantly more purines than pyrimidines. All sequences possess at least one region of four or more consecutive purines (underlined in Fig. 2). In six RNAs (N11, N19, N22, N23, N25, N34), these purine stretches are eight or more nucleotides long. The probability of obtaining such regions by chance is very low. This suggests that these purine-rich parts are functionally important and may be involved in binding the Ni^{2+} ion on the matrix.

Specificity of selected RNAs for different metal ions was tested by affinity elution experiments. Four isolated RNAs (N1, N9, N11, and N32 RNA) were bound to the Ni-NTA resin and eluted with different divalent metal ions. Elution profiles of N1 RNA are shown in Figure 3, and the results of all experiments are summarized in Table 1. A significant portion of the applied sample did not interact with the resin and appeared in the flow-through volume (Fig. 3). The RNA fraction that does not bind to the Ni-NTA matrix may consist of misfolded molecules. A large fraction of the RNA that bound to the resin could be eluted with a buffer containing Ni^{2+} (Table 1). This demonstrates that the selected RNAs do not only interact with immobilized Ni^{2+} on the matrix, but with Ni^{2+} in solution as well. Other divalent metal ions differed strongly in their ability to elute bound RNA. Whereas Co^{2+} was nearly as effective as Ni^{2+}, only a small percentage of RNA was elutable with Mn^{2+}. Virtually no bound RNA could be recovered with Cu^{2+} and Zn^{2+} (Table 1). Therefore, the selected RNAs have a ligand specificity with preference for Ni^{2+} and Co^{2+}.

Dissociation constants and stoichiometry of binding sites

The interaction of two selected RNA molecules, N1 and N11 RNA, with Ni^{2+} in solution was investigated by equilibrium dialysis using the radioactive isotope ^{63}Ni. Experiments were performed in triethanolammo-

```
CLONE #        1          11         21         31         41
                |          |          |          |          |

N1  (6×):  5'- AUAGUCAGGG AACAUGACAA ACACAGGGAC UUGCGAAAAU CAGUGUUUUG -3'
N9  (4×):  5'- GAAACACGAU CAACGGUCAU GACACUGACA CGUUGCUACG GACAAGACA -3'
N10 (2×):  5'- GCACGGCAAA GCUAGAUUAG GCACCAACUC UGUACCCAAA UCAAACACGG -3'
N11 (5×):  5'- GAAAAACCAA CAAAUUGGGA AAAAUGUUAA GGGUCCACUU CAUG -3'
N19 (1×):  5'- CAUGGAUAAU CCAGAAAAGG AGCCUUUACC AAGACCGCAU UCGAGGAUGA -3'
N22 (1×):  5'- UUGAGAGCCG CUAAAAAGGG CGUCUUGGAU UGCGCAUUCU AAAGCU -3'
N23 (2×):  5'- GAAGUGCGCA UUCAAUCAAA AAGGGCUCAC GUGUGAAGGU GUCCCUCUCA -3'
N25 (2×):  5'- AACCGAAUCU CCAAGGGAAA AGCCAUUCCA AAGGGUCCCU GAGAUUGUGG -3'
N28 (1×):  5'- AUAACCACAA AUCAGCCUCG UAAUCUCCGC UGGCAGGGAC UUACGGUUU -3'
N29 (1×):  5'- AACCCAGCAA GCGAAGACAG GGACUUGCAA AAAUCAGUCU GACUUGCCGA -3'
N32 (1×):  5'- GACAGAAAAU CCAGUGCCAC UGUGCCUAAG GGUCUCGAU -3'
N34 (1×):  5'- CCGCCGUAGC AACGGGCAAA AGGAGCCAUG AAAUCUGGCC GCAUUCAG -3'
N40 (1×):  5'- CAGUCGUUUA CUUAGCUAAG GGUCGACAUG AAAAGCCAGA CUAAGUCCCA -3'
```

FIGURE 2. Sequences of the selected Ni^{2+}-binding RNA molecules. The PCR product corresponding to the RNA of the eighth selection-amplification cycle was cloned, and 28 clones were sequenced. Only the sequence corresponding to the originally randomized nucleotides is shown. The number of identical clones in the sequenced pool is indicated in parentheses. Stretches of four or more consecutive purines, supposed to be involved in Ni^{2+} binding, are underlined.

nium acetate at pH 5.7 in the absence of other monovalent or divalent cations. Similar conditions have been used earlier to study the interaction of Mn^{2+} and tRNA (Danchin, 1972; Schreier & Schimmel, 1974). The large radius of the triethanolammonium cation reduces its competitive binding to functional groups of the RNA. A slightly acidic pH was chosen because higher pH can result in the formation of aggregates of divalent metal ions. Furthermore, at lower pH, the rate of RNA degradation is reduced.

The Scatchard plot for the interaction of Ni^{2+} with N11 RNA (Fig. 4) has a positive slope for $r < 1$ and is curved for $r > 1$, with r representing the number of bound Ni^{2+} per RNA molecule. Similar positive cooperativity had also been observed for Mn^{2+} binding to tRNA (Danchin, 1972; Schreier & Schimmel, 1974) and was interpreted as a divalent metal ion-induced conformational change of the RNA. The curved part of the Scatchard plot ($r > 1$) indicates the existence of two or more classes of Ni^{2+} binding sites with different dissociation constants (K_d). It can be interpreted most easily if only two types of binding sites are assumed. The steep part would reflect interaction of Ni^{2+} with strong binding sites, whereas the part with the shallow slope would represent binding to weak sites. On the basis of this model, the individual plots corresponding to the two classes of binding sites were determined by a graphic method (Rosenthal, 1967). The K_d for binding of Ni^{2+} to the weak binding sites is given by the slope of the straight line for $r > 9$ (Fig. 4). Different numbers of weak binding sites were assumed, and the partial plot for the strong binding sites was constructed accordingly. The best fit, with the points for the strong binding being on a straight line, was obtained when assuming 15 weak binding sites. This plot gives between one and two strong binding sites with a K_d of less than 1 μM, compared to the K_d for binding to the weak sites, which is about 35 times higher (Table 2).

The Scatchard plot for the interaction of Ni^{2+} with N1 RNA showed essentially the same characteristics as that of N11 RNA: positive slope for $r < 1$ and curvature for $r > 1$ (data not shown). The curved part was also analyzed assuming two classes of binding sites. This results in one strong binding site, with a K_d of about 1 μM, and 12 weak binding sites (Table 2). The measurements of the Ni^{2+} interaction with N1 and N11 RNA demonstrate that the molecules have strong binding sites for Ni^{2+}, with a K_d in the low-micromolar range. The strong binding sites probably determine the interaction of the RNAs with immobilized Ni^{2+}. It is very likely that N11 RNA contains only one strong binding site, because statistically it is nearly impossible to select two ligand binding motifs within one randomized sequence. Interaction of Ni^{2+} with the weak

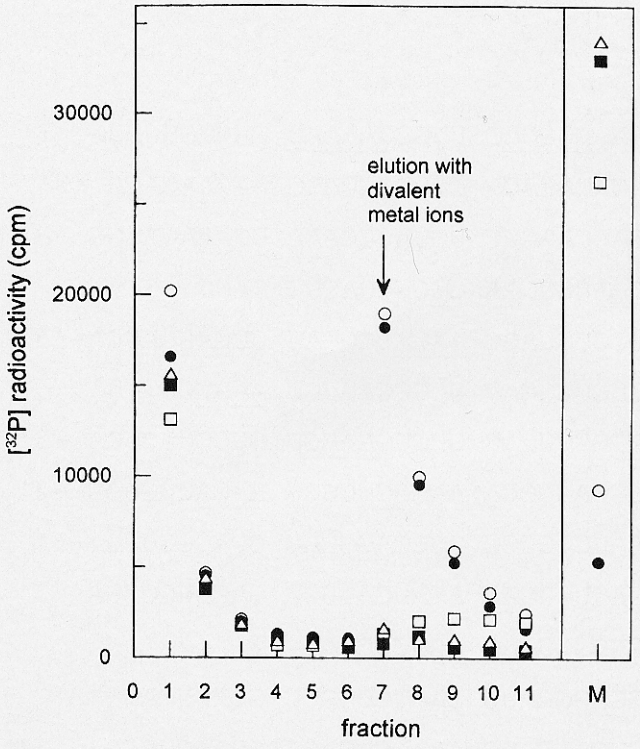

FIGURE 3. Elution profiles of N1 RNA. Internally [^{32}P]-labeled RNA (12.5 μg) in 100 μL buffer A was bound to 100 μL Ni-NTA resin for 5 min. Unbound RNA was removed by centrifugation (fraction 1) and the matrix was washed with five times 300 μL buffer A (fractions 2–6). Bound RNA was then eluted from the resin with five times 100 μL buffer A containing 100 mM $NiCl_2$ (○), 100 mM $CoCl_2$ (●), 100 mM $MnCl_2$ (□), 100 mM $CuCl_2$ (■), or 100 mM $ZnCl_2$ (△); (fractions 7–11). Counts in fraction "M" correspond to radioactivity that remained bound to the matrix.

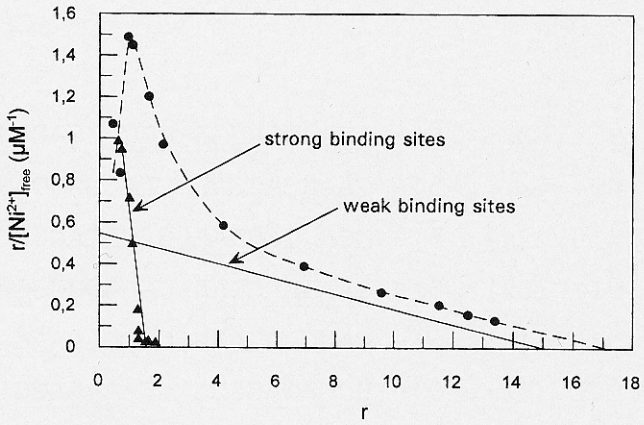

FIGURE 4. Scatchard plot for the binding of Ni^{2+} to N11 RNA. $[Ni^{2+}]_{free}$ is the concentration of unbound Ni^{2+}, and r the ratio $[Ni^{2+}]_{bound}/[RNA]$. Assuming two classes of Ni^{2+} binding sites, analysis of the curved part of the Scatchard plot ($r > 1$) was performed according to Rosenthal (1967), and the partial plots for Ni^{2+} binding to the weak (——) and strong (—▲—) sites were constructed from the measured curve (– – –●– – –). Individual plots yield the dissociation constant and number of binding sites as the slope and intercept with the horizontal axis, respectively (Table 2).

binding sites of the RNAs probably reflects a rather unspecific neutralization of negative charges and is due to the absence of Na^+ and Mg^{2+} in the equilibrium dialysis experiments.

Structures of the selected RNAs

Secondary structures were calculated for the isolated RNAs according to algorithms developed by Zuker (1989). Comparison of the resulting secondary structures revealed several conserved motifs. These motifs (Fig. 5A) are present in N1, N28, and N29 RNA (motif I), N25 and N40 RNA (motif II), N19 and N34 RNA (motif IIIa), and N22 and N23 RNA (motif IIIb). The conserved regions comprise about 15 nt and contain a stretch of consecutive purines (boldface in Fig. 5A). An internal loop is located in all motifs that is asymmetric in the case of motifs I and II and consists only of purines. As an additional common feature, formation of a mismatch G-A base pair at the junction of internal loop and helix seems possible.

In the calculated secondary structure of N1 RNA, which is the most abundant RNA in the sequenced pool, a long helix that involves base pairing of both primer binding sites ends in a three-helix junction from which two hairpins originate (Fig. 5B). The conserved motif I is located in the large 3′-hairpin domain (A40–U67). This secondary structure was confirmed by cleavage of N1 RNA with single strand-specific nuclease S1 (Figs. 5B, 6A) Under applied conditions (5 mM Zn^{2+}, absence of Mg^{2+}), the S1 nuclease cuts preferentially at positions where loops were predicted by thermodynamic calculations. Minimal structural elements of

TABLE 1. Fraction of RNA eluted from the Ni-NTA resin with different divalent metal ions.[a]

	Ni^{2+}	Co^{2+}	Mn^{2+}	Cu^{2+}	Zn^{2+}
N1 RNA	+++	+++	+	–	–
N9 RNA	++	+++	+	–	–
N11 RNA	++	+	–	–	–
N32 RNA	++	++	–	–	–

[a]Percentage of the total bound RNA that could be eluted was determined in experiments described in Figure 3. –, 0–10% eluted; +, 11–50% eluted; ++, 51–80% eluted; +++, 81–100% eluted.

TABLE 2. Number of Ni^{2+} binding sites (n) and dissociation constants (K_d) for the interaction of Ni^{2+} with N1 RNA and N11 RNA as determined by analysis of the Scatchard plots (Scatchard, 1949).

	Strong sites	Weak sites
N1 RNA	$n = 1$	$n = 12 \pm 1$
	$K_d = 1$ μM	$K_d = 26$ μM
N11 RNA	$n = 1$–2	$n = 15 \pm 1$
	$K_d = 0.8$ μM	$K_d = 29$ μM

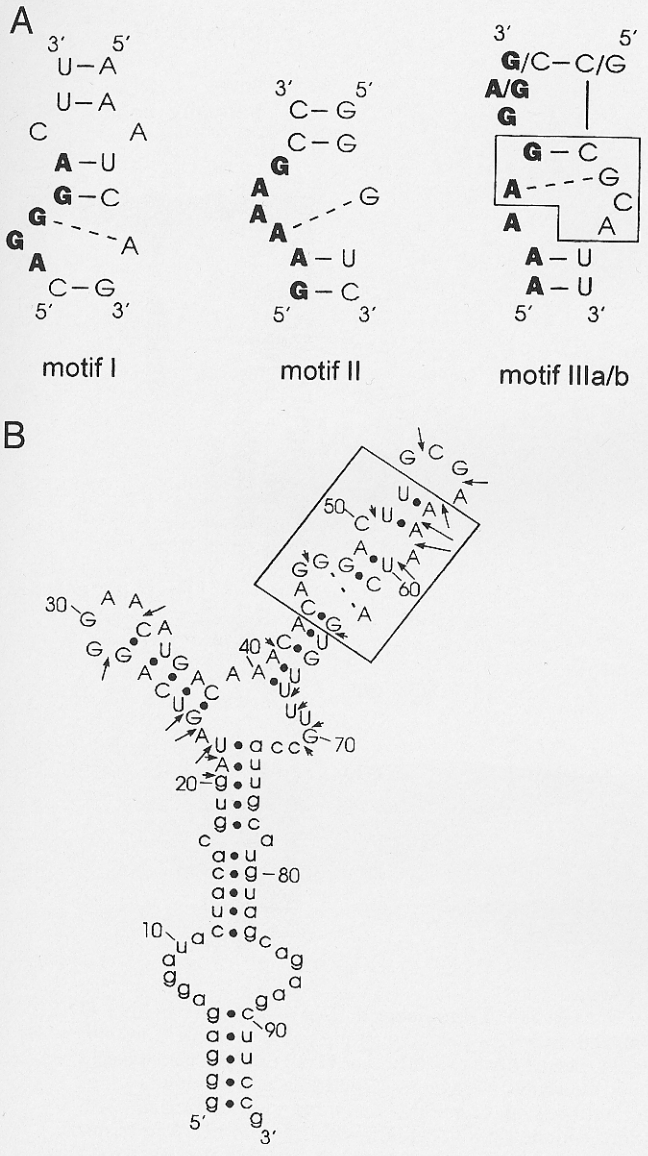

FIGURE 5. Secondary structures of Ni^{2+}-binding RNAs. **A:** Conserved secondary structure motifs identified in N1, N28, and N29 RNA (motif I), N25 and N40 RNA (motif II), N19 and N34 RNA (motif IIIa), and N22 and N23 RNA (motif IIIb), respectively. Stretches of consecutive purines are in boldface type (compare with Fig. 2), proposed G-A base pairs are indicated with broken lines. The boxed part in motif IIIa/b is present in an in vitro-selected Zn^{2+}-binding RNA motif also (Ciesiolka & Yarus, 1996). The structure depicted as motif I consisting of two oligonucleotides extended by additional residues was used for NMR measurements shown in Figures 7 and 8. **B:** Secondary structure prediction for N1 RNA. Nucleotides in the region originally randomized are depicted with capital letters, small letters symbolize the primer binding sites, the boxed part represents the conserved motif I (see A). Nuclease S1 cuts (Fig. 6A) are marked with arrows; the length of the arrow corresponds to the intensity of cleavage. 3′-boundary (○—) and 5′-boundary (>——) were obtained by testing partially hydrolyzed end-labeled molecules for binding to the Ni-NTA resin (Fig. 6B).

an RNA sufficient for binding a ligand can be determined by progressive deletion of the 5′ end and 3′ end. Boundaries that mark the minimal lengths at either end are located in N1 RNA at both ends of the partly conserved 3′-hairpin (Figs. 5B, 6B), demonstrating that this domain represents the minimal binding motif. The Ni^{2+} binding site is probably located in the conserved motif I. The adjacent double-stranded part (A40–A43 base pairing with U64–U67) and the tetraloop, G53–A56, may serve to stabilize the binding site.

Proton NMR spectra and UV melting curves of a Ni^{2+}-binding motif

Proton NMR spectroscopy was applied to study the structure and divalent metal ion binding capability of conserved motif I, which was shown to be located in the minimal Ni^{2+}-binding domain of N1 RNA. For NMR measurements, motif I was stabilized by the attachment of additional base pairs and a 3′-dangling G residue at the helix ends (Fig. 7). This molecule was synthesized chemically and demonstrated to be still able to bind to the Ni-NTA resin (data not shown).

The imino proton resonances in the downfield region of the proton NMR spectrum of motif I (Fig. 7) reflect the proposed secondary structure. The imino signals are sharp and well resolved and were assigned to the individual base pairs by nuclear Overhauser effect (NOE) measurements and analysis of the temperature-dependent changes of the NMR spectrum. The resonance at 11.93 ppm was assigned to the imino proton of G7, which forms a mismatch base pair with A23. This value corresponds very well to findings of SantaLucia et al. (1990), who observed a chemical shift of 11.97 ppm for an imino hydrogen bonded G-A base pair in the same sequence context (5′-CA-3′/3′-GG-5′).

The binding of a paramagnetic metal ion can accelerate the relaxation of the nuclear spin of protons near the binding site, which results in a broadening of the corresponding resonances. This effect decreases with the sixth power of the distance between the paramagnetic ion and the proton. Broadening is therefore restricted to protons that are bound within a radius of about 10 Å of the paramagnetic ion (Craik & Higgins, 1989). Ni^{2+} can form complexes with four electron pairs or complexes with three electron pairs and two unpaired electrons, depending on the specific ligands and the coordination geometry. In octahedral complexes, Ni^{2+} almost exclusively occurs in the "high spin" form, with two unpaired electrons, and hence is paramagnetic. Up to now, Ni^{2+} has not been employed as a paramagnetic probe in NMR studies of RNA molecules. It has been used in the characterization of metal-binding proteins, where it caused specific paramagnetic alterations of chemical shifts (Moratel et al., 1991; Salgado et al., 1996).

The effect of addition of increasing amounts of Ni^{2+} on the imino proton NMR spectrum of the stabilized motif I is shown in Figure 8. At 0.2 mM Ni^{2+}, a specific linewidth increase of the G7–A23 imino proton resonance at 11.93 ppm is detected (Table 3). An increase of

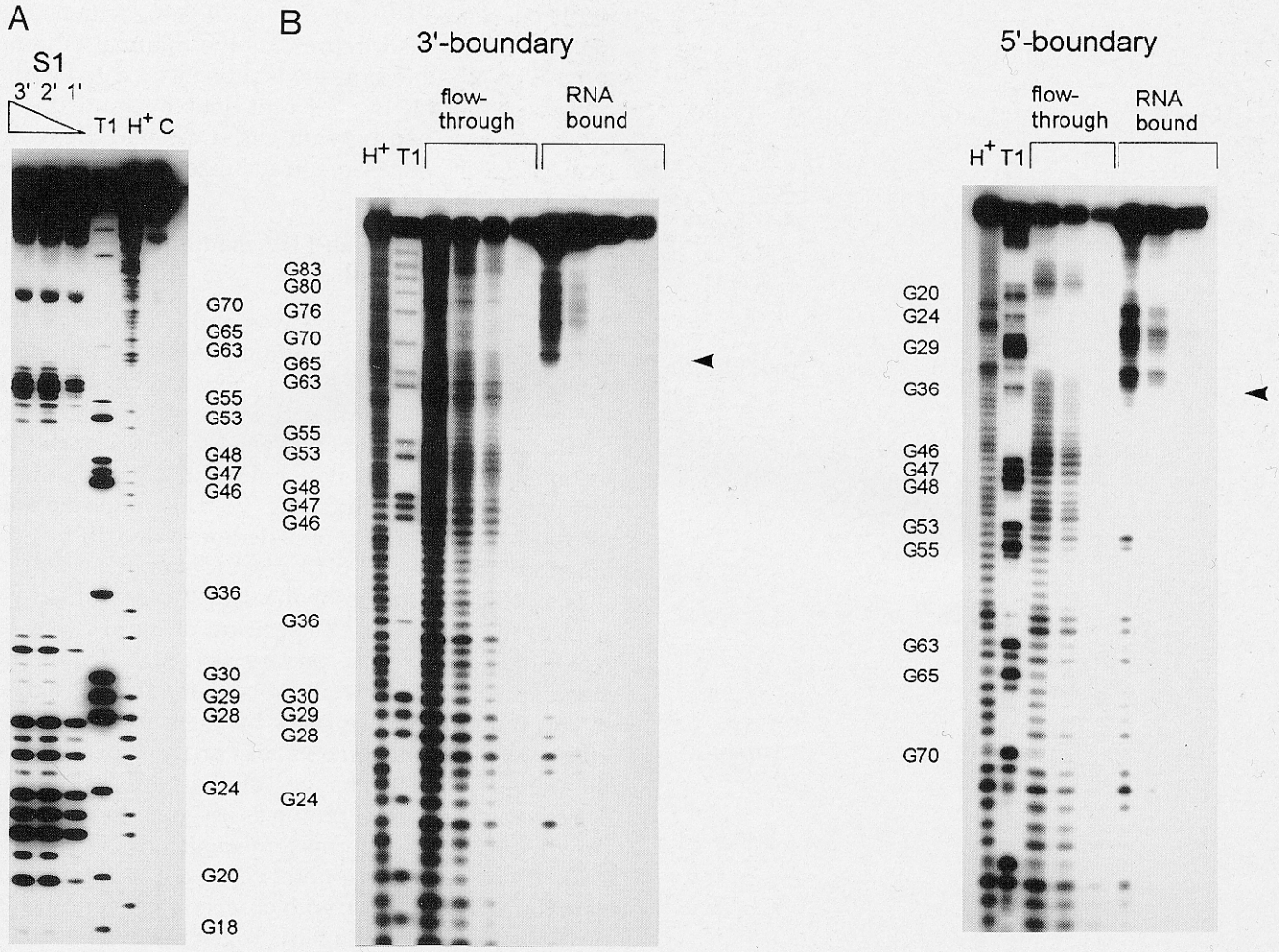

FIGURE 6. Probing of the structure of N1 RNA. **A:** Nuclease S1 cleavage. 5′-End-labeled RNA was treated with 1 U nuclease S1 for various incubation times (1, 2, 3 min) and analyzed on a 12% polyacrylamide gel. C, control lane with untreated RNA; H^+, limited hydrolysis under acidic conditions; T1, partial digest with RNase T1. **B:** Boundary analysis to determine the sequences of the RNA important for Ni^{2+} binding. Molecules were either 5′-end-labeled (3′-boundary), or 3′-end-labeled (5′-boundary), partially digested under alkaline conditions, and separated on Ni-NTA resin. Fractions with RNA that did not bind to the matrix (flow-through), and fractions containing RNA eluted with 100 mM EDTA in buffer A (RNA bound) were collected and analyzed on a 12% polyacrylamide gel. Boundary positions are indicated by arrowheads.

the Ni^{2+} ion concentration to 1 mM causes very strong broadening of the line corresponding to the G-A pair as well as of the one due to base pair **8**, so that they are no longer detectable in the spectrum. Moreover, the lines originating from the imino protons of base pairs **7**, **9**, and **10** appear likewise to be broadened extensively. The line broadening is not restricted to the imino proton region, and can be detected in the aromatic proton region, too (data not shown).

The broadening of distinct imino proton signals at different Ni^{2+} concentrations indicates that there is probably more than just one Ni^{2+} binding site. From the specific linewidth increase of the imino proton signal of the G7–A23 base pair at 0.2 mM Ni^{2+}, an initial occupation of a binding site close to this mismatch pair is suggested. Upon the Ni^{2+} addition, the resonance due to the adjacent base pair **6** appears to be almost unaffected, whereas, at the same time, the broad line at ca. 10.5 ppm, which possibly originates from loop nucleotide G6, vanishes. This suggests a strong Ni^{2+} binding site located in the internal loop of motif I (Fig. 7). At 1 mM Ni^{2+}, the imino signals of base pairs **7–10** are strongly broadened. This leads to the postulation of a second, low-affinity Ni^{2+} binding site in this nonconserved part of the stabilized motif I near the consecutive purines G1–A3 (Fig. 7). This interpretation is compatible with previous observations that demonstrated the ability of consecutive purines in double-stranded RNA regions to form specific binding sites for divalent metal ions (Rubin et al., 1983; Ott et al., 1993; Allain & Varani, 1995; Scott et al., 1995).

The existence of the two divalent metal ion binding sites is further corroborated by NMR studies of the effect of paramagnetic Mn^{2+} on the stabilized motif I

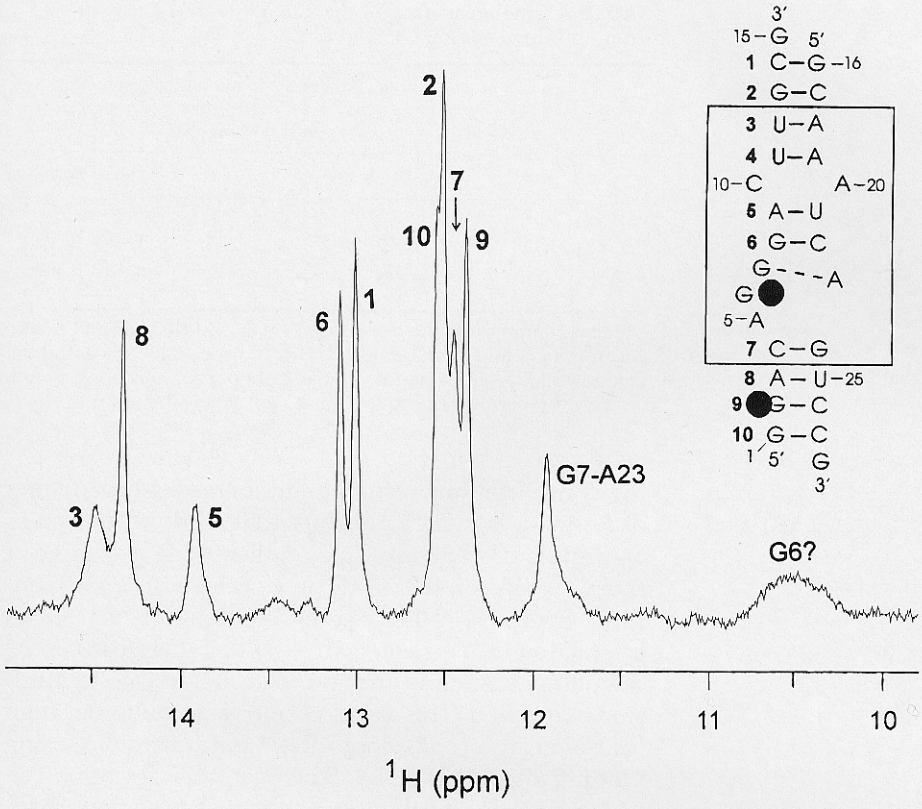

FIGURE 7. Imino proton region of the NMR spectrum of motif I. The conserved part (boxed) was stabilized by the attachment of additional base pairs and 3′-dangling guanosines. Nucleotides and standard base pairs are numbered. The spectrum was measured at 3 °C in 100 mM NaCl, 10 mM sodium phosphate, pH 6.5. Assignment of the imino proton resonances to the individual base pairs is indicated. The signal at 11.93 ppm represents the imino proton of the mismatch base pair G7–A23, the broad line at ca. 10.5 ppm possibly originates from loop nucleotide G6. The approximate positions of divalent metal ion binding sites, derived from the line broadening effects of paramagnetic Ni^{2+} (Fig. 8; Table 3), are marked with black circles.

(data not shown). However, both the specificity and the affinity of these binding sites for Mn^{2+} are distincly lower than for Ni^{2+} ions, as should be expected for an RNA motif that has been selected for Ni^{2+} binding.

UV melting curves at different Ni^{2+} concentrations were measured to study the influence of Ni^{2+} on the stability of the stabilized motif I. The melting transition is at least biphasic (Fig. 9), which indicates the existence of one or more intermediates. The temperature-dependent changes of the imino proton NMR spectrum of the motif I (data not shown) demonstrate that the double-stranded part, which is formed by base pairs **7–10**, seems to be more stable than the rest of the molecule. This could account for the observed melting behavior. Melting temperatures (T_m) were determined for the whole transition. The addition of Ni^{2+} led to a significant increase of the T_m. Surprisingly, the T_m of stabilized motif I RNA in the presence of 300 μM Ni^{2+} has approximately the same value as in the presence of 5 mM Mg^{2+} (see inset of Fig. 9). This result is in contrast to previous studies by Eichhorn and Shin (1968) on the influence of divalent metal ions on the stability of DNA, in which Mg^{2+} was more stabilizing than Ni^{2+}. This indicates that Ni^{2+} exerts a specific stabilization effect on motif I that might be caused by its association with the strong Ni^{2+} binding site. It is clear, however, that the structures in the presence of different divalent ions may differ from each other.

DISCUSSION

There is one strong binding site for Ni^{2+} on N1 RNA and N11 RNA with a dissociation constant of about 1 μM. For binding of Mg^{2+} or Mn^{2+} to the strong binding sites on tRNAs, dissociation constants in the range of 1–10 μM were measured under experimental conditions comparable to those used in the present study (Danchin, 1972; Schreier & Schimmel, 1974; Schimmel & Redfield, 1980). The dissociation constants were significantly higher, 10–50 μM, when the metal ion-tRNA binding was studied in the presence of about 100 mM of Na^+ (Schimmel & Redfield, 1980). The dissociation constants for the interaction of Zn^{2+} and the recently selected Zn^{2+}-binding RNA aptamers were 100–400 μM (Ciesiolka & Yarus, 1996). This value is about 100-fold higher than the K_d for the Ni^{2+}-binding RNA aptamers described here. However, the two results are difficult to compare because the Zn^{2+}–RNA interaction was studied in the presence of a high concentration of competing Na^+ and Mg^{2+} ions.

The selected RNA molecules show a ligand specificity with preference for Ni^{2+} and Co^{2+} over other metal ions of the first transition series, Mn^{2+}, Cu^{2+}, and Zn^{2+}. This specificity seems to follow the order, $Mg^{2+} < Co^{2+}$, $Ni^{2+} < Mn^{2+} < Zn^{2+} < Cd^{2+} < Cu^{2+}$, in which divalent metal ions were arranged according to their relative affinities for phosphate and nucleobase resi-

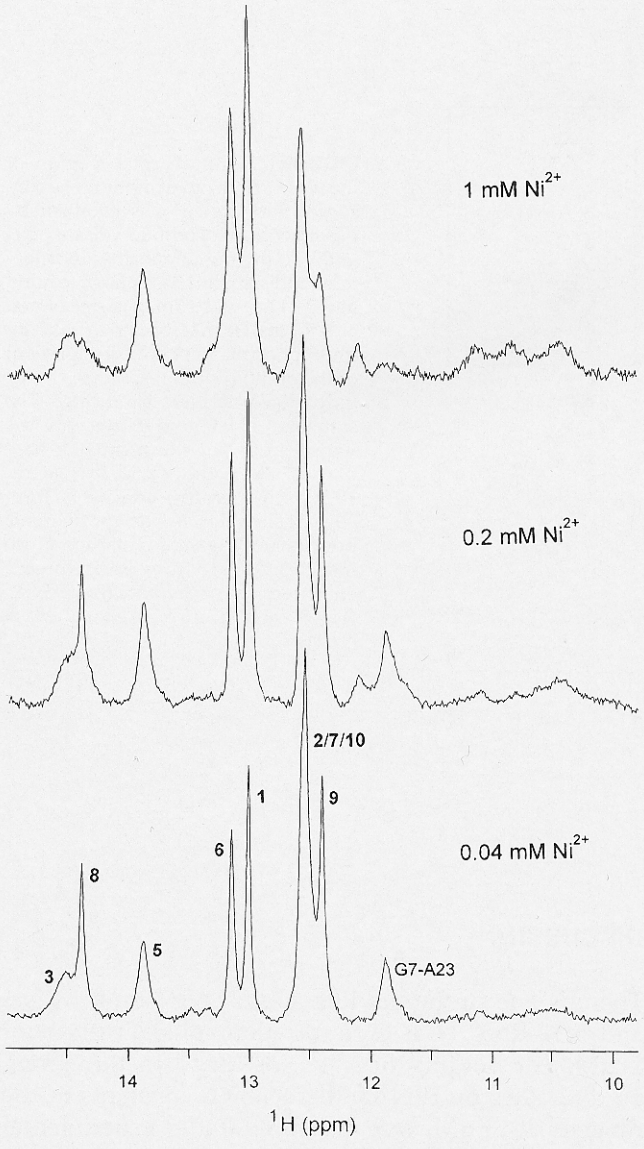

FIGURE 8. Effect of Ni^{2+} on the imino proton NMR spectrum of motif I. Spectra were measured in 100 mM NaCl, 5 mM $MgCl_2$, 10 mM sodium phosphate, pH 6.5, in the presence of increasing concentrations of $NiCl_2$ as indicated in the spectra.

TABLE 3. Line broadening of the imino proton resonances of motif I upon adding Ni^{2+}.

	$\Delta\Delta\nu_{1/2}$ (Hz) of the imino proton resonance[a]					
	Base pair number[b]					
	8	5	6	1	9	G7–A23
0.04 mM Ni^{2+}	1, 5	9	3, 5	−2, 5	0	13
0.2 mM Ni^{2+}	6, 5	12, 5	5	2, 5	2, 5	31, 5
1 mM Ni^{2+}	n.d.	30	22	9	n.d.	n.d.

[a] $\Delta\Delta\nu_{1/2}$ represents the difference of half widths after and before addition of 5 mM $MgCl_2$ and Ni^{2+} in the specified concentration. Due to overlap of resonances, not all base pairs could be analyzed.
[b] For numbering, see Figure 7; n.d., not determinable.

dues in DNA (Eichhorn & Shin, 1968). Ni^{2+} and Co^{2+} were virtually indistinguishable in that study. The specificity of the Ni^{2+}-binding RNA species described here appears to be higher than the ligand specificity of a selected Zn^{2+}-binding RNA, which has a preference for binding Zn^{2+}, Ni^{2+}, Co^{2+}, and Cd^{2+} stronger than Ca^{2+} and Mn^{2+} (Ciesiolka et al., 1995).

The paramagnetic line broadening in the imino region of the proton NMR spectrum of the RNA duplex derived from motif I at different Ni^{2+} concentrations suggests the existence of two distinct binding sites for Ni^{2+}. One of them, the strong Ni^{2+} binding site, is located close to the G7–A23 mismatch pair. The other Ni^{2+} binding site is formed by a stretch of three consecutive purines (G1–A3). The addition of Ni^{2+} in rising concentrations results in an increased broadening of resonances, which indicates that all RNA molecules are influenced equally. This implies a fast exchange of the Ni^{2+} ions on the NMR time scale, with a rate constant $>10^3$ s^{-1}. A dissociation constant for Ni^{2+}-RNA interaction in the range >10–100 μM therefore can be calculated assuming that the association rate is diffusion controlled. This value is significantly higher than the dissociation constant for Ni^{2+} binding to the strong binding site of N1 RNA. However, this deviation can be explained with the competition of Na^+ and Mg^{2+} ions for the Ni^{2+} binding site in the NMR studies. Compared to Mn^{2+}, which is used commonly as a paramagnetic probe in NMR investigations of metal ion–RNA interactions (Ott et al., 1993; Allain & Varani, 1995), the paramagnetic effects of Ni^{2+} on motif I are more distinct. Addition of Ni^{2+} to motif I led to a strong broadening or complete disappearance of certain imino resonances, whereas other signals remained unaffected. Mn^{2+}, in contrast, resulted in less specific broadening of all lines (data not shown). This demonstrates that Ni^{2+} is well suited as a paramagnetic probe and should be an interesting alternative to Mn^{2+} in NMR studies of metal ion binding to RNA.

Involvement of two or more consecutive purines in double-stranded RNA in binding of divalent metal ions has been shown by X-ray crystallography (Rubin et al., 1983; Scott et al., 1995) and NMR (Ott et al., 1993; Allain & Varani, 1995). Coordination of the metal ion characteristically occurs to adjacent purine N7 nitrogens. The second metal ion binding site that was identified in the nonconserved part of stabilized motif I obviously represents this type of binding. Participation of G-U base pairs in coordination of divalent metal ions has also been suggested (Ott et al., 1993; Allain & Varani, 1995). In the central core of the hammerhead ribozyme, a Mn^{2+} or Mg^{2+} ion was localized near two consecutive G-A base pairs (Pley et al., 1994; Scott et al., 1995). The motif 5′-GAR-3′/3′-AG-5′ was therefore suggested as a divalent metal ion binding site (Pley et al., 1994). RNA motifs with high affinity for Zn^{2+} have been isolated recently by in vitro selection

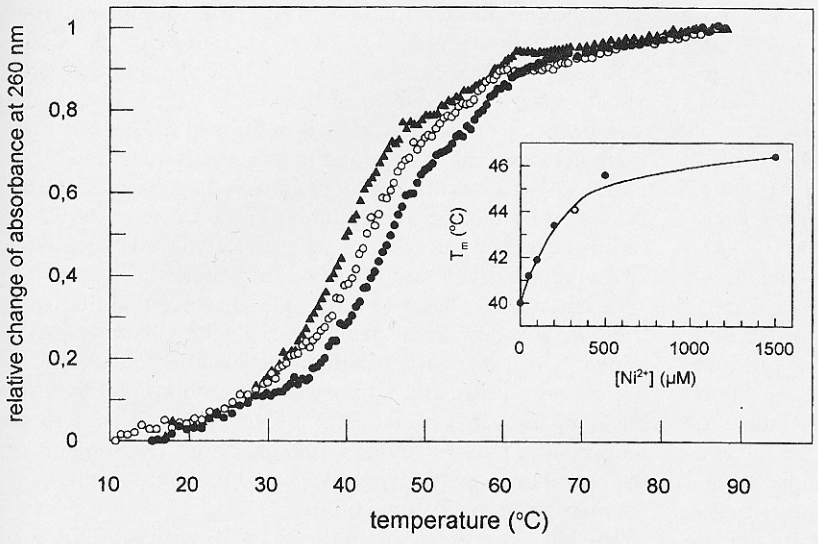

FIGURE 9. UV melting curves of stabilized motif I (Fig. 7). Normalized absorbance of 1.5 μM RNA in 100 mM NaCl, 10 mM sodium phosphate pH 6.5 with 0 μM (▲), 100 μM (○), and 500 μM (●) $NiCl_2$ is plotted versus temperature. In the inset, the dependence of the melting temperature (T_m) of the RNA on the Ni^{2+} concentration is shown (filled circles); the increase of T_m upon addition of 5 mM $MgCl_2$ is marked with an open circle.

(Ciesiolka & Yarus, 1996). One of the motifs, which contains a G-A base pair and a C-A mismatch, was called E element due to its similarity to the E-loop motif of RNA (Wimberly, 1994). Other selected Zn^{2+}-binding motifs consist of consecutive G-C base pairs (GC cluster) and additional conserved elements that were postulated to increase the Zn^{2+} affinity. In one of these so-called augmented GC clusters, a G-A pair and a partly conserved 3-nt bulge are located adjacent to the G-C stretch (Ciesiolka & Yarus, 1996). The conserved motifs in the Ni^{2+}-binding RNAs isolated in this work consist of about 15 nt and are surprisingly large, when one takes into account that only a small number of functional groups should be involved directly in coordinating the metal ion. A part of motif IIIa/b, which comprises six nucleotides, is also found in one of the augmented GC clusters for Zn^{2+} binding (Ciesiolka & Yarus, 1996; see Fig. 5A). Motifs I and II (Fig. 5A) contain small asymmetric internal loops that consist only of purines. The binding of Ni^{2+} to the loop region of motif I was deduced from broadening of NMR resonances. These purine-rich internal loops represent a novel structural element for binding of divalent metal ions. Such elements may be useful to predict metal ion binding sites in other RNA molecules.

The G7–A23 interaction in motif I was derived from proton NMR measurements. G-A pairs in RNA can have different structures. The sheared conformation, which was observed, for example, in loop E of eukaryotic 5S rRNA (Wimberly et al., 1993) and in the core of the hammerhead ribozyme (Pley et al., 1994; Scott et al., 1995), includes hydrogen bonding of G-N2H to A-N7, and G-N3 to A-N6H. In contrast, the G-N1H imino proton is directly involved in hydrogen bonding in an alternative structure that was identified in a self-complementary dodecamer (Leonard et al., 1994) and octamer (Wu & Turner, 1996). Here, hydrogen bonds of G-N1H to A-N1, and G-O6 to A-N6H are formed. These differences in hydrogen bonding geometry are reflected in the imino proton NMR spectrum (Limmer, 1997). A broader imino proton signal upfield-shifted from ca. 11 ppm appears if the guanosine imino proton does not participate in a hydrogen bond. In contrast, involvement of the imino proton in a base pair hydrogen bond gives rise to a sharper resonance downfield from ca. 11 ppm. The signal of G7–A23 in motif I is observed at 11.93 ppm and is comparatively sharp. This indicates that the base pair has a structure in which the guanosine imino proton is hydrogen bonded, similar to the G-A base pair geometry recently characterized by Wu et al. (1997) by NMR.

It has been proposed that the variety of RNA-catalyzed reactions can be increased by using metal ion cofactors with different properties (Yarus, 1993). Ni^{2+} is a cofactor in urease, a protein enzyme that catalyzes the hydrolysis of urea. The crystal structure of the enzyme supports a reaction mechanism in which two Ni^{2+} ions participate directly in activation and hydrolysis of the substrate (Jabri et al., 1995). This suggests that reactions at amide bonds, e.g., a peptide cleavage, might be catalyzed by Ni^{2+}-containing ribozymes particularly well. RNA binding motifs that occupy only some of the coordination sites of the Ni^{2+} ion may help to engineer such ribozymes (Ciesiolka & Yarus, 1996).

MATERIALS AND METHODS

Selection-amplification cycle

The double-stranded DNA template for transcription with bacteriophage T7 RNA polymerase was made by PCR amplification of the chemically synthesized single-stranded DNA template 5′-CGGAAGCTTCTGCTACATGCAATGG$(N)_{50}$CACGTGTAGTATCCTCTCCC-3′, where $(N)_{50}$ is a randomized region of 50 nt. The sequence of the 5′ primer (forming base pairs with the 3′ primer binding site of the template) was

5′-GCGAATTCTAATACGACTCACTATAGGGAGAGGAT ACTACACGTG-3′, and 5′-CGGAAGCTTCTGCTACATGCA ATGG-3′ was used as a 3′ primer. The T7 promoter is in boldface type, the restriction sites for cloning (*Eco*R I and *Hin*d III) are underlined.

PCR reactions were performed in 50 mM KCl, 1.5 mM $MgCl_2$, 0.1% Triton X-100, 10 mM Tris/HCl, pH 9.0, with dNTPs (0.2 mM each), 0.75 μM 5′ primer and 3′ primer, and 2.5 U Taq DNA polymerase (MBI Fermentas) per 100 μL reaction. Transcription with T7 RNA polymerase was performed in 40 mM Tris/HCl, pH 8.1, 22 mM $MgCl_2$, 5 mM dithioerythritol, 1 mM spermidine, 0.01% Triton X-100, 4 mM of each NTP, in a final volume of 100 μL; the product of 1.5 PCR reactions was used as a template. After addition of T7 RNA polymerase and [α-^{32}P] GTP for internal labeling, the reaction proceeded for approximately 4 h at 37 °C. The transcription product was analyzed by PAGE under denaturing conditions (7 M urea). In most cases, the product was sufficiently pure to be used without further purification. Unincorporated nucleotides were removed by gel permeation chromatography on Sephadex G-50 (Pharmacia) followed by the degradation of the template in 6 mM $MgCl_2$, 40 mM Tris/HCl, pH 7.5 with 30 U DNaseI (Pharmacia) for 1 h at 37 °C.

RNA selection was performed on Ni-NTA resin (Qiagen; Fig. 1), which contains 8–12 μmol Ni^{2+}/mL resin according to the manufacturer's specification. The selection was performed in a batch procedure in 1.5-mL Eppendorf tubes with repeated mixing and centrifugation steps. Ni-NTA resin (200 μL) was equilibrated with a buffer that contained 50 mM NaCl, 7 mM $MgCl_2$, 50 mM Tris/HCl, pH 7.5 (buffer A). An aqueous solution of RNA (50 μg, 6×10^{14} molecules, 10^{13}–10^{14} different molecules in cycle 1) was heated at 75 °C for 3 min and then slowly cooled to room temperature. Salt and buffer were added to yield the RNA in buffer A in a total volume of 200 μL. The sample was loaded on the Ni-NTA matrix for 5 min under gentle agitation. Unbound RNA was removed by centrifugation, and the resin was washed with seven times 600 μL buffer A. Then the matrix was washed in five successive steps with 200 μL buffer A with 100 mM imidazole. During each elution step, the material was gently agitated for 5 min, then the solution was removed by centrifugation. RNA eluted with imidazole was precipitated with ethanol in the presence of glycogen (20 μg/mL) and reverse transcribed in two 20-μL reaction mixtures with 50 mM Tris/HCl, pH 8.7, 40 mM KCl, 6 mM $MgCl_2$, 0.5 mM dNTPs, 3.75 μM 3′ primer, and 40 U AMV reverse transcriptase (Life Sciences). PCR amplification of the cDNA and transcription of the PCR product with T7 RNA polymerase resulted in an RNA pool used for the next selection-amplification cycle. After enrichment of the RNA pool for molecules binding to the Ni-NTA resin, the corresponding PCR product was cleaved with *Eco*R I and *Hin*d III and cloned in pUC 19. Individual clones were sequenced using the "T7 sequencing Kit" (Pharmacia).

Determination of equilibrium dissociation constants

The dissociation constants (K_d) for the interaction of Ni^{2+} with selected RNAs and the binding stoichiometries were determined by equilibrium dialysis using the radioactive isotope ^{63}Ni, which decays by β emission with an energy of 0.067 MeV and a half-life of 92 years. The equilibrium dialysis chambers (volume 40 μL) were separated by SPECTRA/POR dialysis membranes (Spectrum Medical Industries) with a molecular weight cut-off of 6,000–8,000. Prior to use, the membranes were heated for 1 h in 50 mM EDTA and then washed extensively with water to remove all traces of EDTA. The RNA was desalted on Sephadex G-50 (Pharmacia) and recovered by ethanol precipitation in the presence of 0.3 M sodium acetate, pH 6.5. The pellet was washed twice with 70% ethanol, dried, and dissolved in water.

In chamber 1, RNA (5 μM) was dissolved in 100 mM triethanolammonium acetate buffer, pH 5.7. Chamber 2 contained 1.18 μM $^{63}NiCl_2$ (DuPont de Nemours; 12.28 mCi/mg, 9.73 mCi/mL) and different concentrations of unlabeled $NiCl_2$ in the same buffer. The dialysis proceeded at room temperature for 20 h under gentle agitation. The contents of the chambers were then removed, and the radioactivity was counted in a scintillation counter.

The Ni^{2+} concentration in the chamber without RNA corresponds to the concentration of unbound Ni^{2+} ($[Ni^{2+}]_{free}$). The difference in counts between the chamber with and without RNA corresponds to the concentration of bound Ni^{2+} ($[Ni^{2+}]_{bound}$). Data were analyzed by the method of Scatchard (1949), where $r/[Ni^{2+}]_{free}$ ($r = [Ni^{2+}]_{bound}/[RNA]$) is plotted versus r. The curve yields $-1/K_d$ as the slope and n, the number of Ni^{2+} binding sites on the RNA molecule, as the intercept with the horizontal axis.

Deletion of 5′ ends and 3′ ends (boundary analysis)

In order to determine the regions of selected RNA that are important for Ni^{2+} binding, 5′ deletions and 3′ deletions were performed. RNA was either 5′-end-labeled with polynucleotide kinase and [γ-^{32}P] ATP, or 3′-end-labeled using T4 RNA ligase and [5′-^{32}P] pCp. Approximately 2 pmol labeled RNA were partially digested in 50 mM sodium carbonate, pH 9.0, 1 mM EDTA at 90 °C for 15 min. After adding 7.5 μg unlabeled RNA and sodium acetate, pH 5.2, to a final concentration of 0.3 M, the sample was precipitated with ethanol. The RNA was annealed by heating to 75 °C and slowly cooling to room temperature and applied to 50 μL Ni-NTA resin. Unbound RNA was eluted with buffer A; the bound RNA was eluted with 100 mM EDTA in buffer A. RNA in separate fractions was precipitated with ethanol, redissolved in 4 μL water and 3 μL gel loading buffer (50 mM EDTA, 0.1% dyes, 88% formamide), and analyzed on a 12% polyacrylamide gel. In order to follow the sequence, a partial digest with RNase T1 (which cleaves on the 3′ side of guanosine residues), as well as a limited hydrolysis under acidic conditions, was run in parallel on the same gel. RNase T1 cleavage of approximately 0.1 pmol RNA was performed with 1 U enzyme in 7 M urea, 1.6 mM EDTA, 32 mM sodium citrate, pH 3.5, for 5 min at 50 °C; the reaction was terminated by adding gel loading buffer. The acid hydrolysis of 0.15 pmol RNA was performed in 7 M urea, 0.11 M H_2SO_4 for 3 min at 90 °C and was stopped by freezing on dry ice.

Nuclease S1 cleavage

Approximately 0.4 pmol 5′-[^{32}P]-labeled RNA and 1 μg *Escherichia coli* $tRNA^{bulk}$ was dissolved in 5 μL of 50 mM NaCl,

5 mM $ZnCl_2$, 5% glycerin, 30 mM sodium acetate, pH 5.0, and incubated with 1 U nuclease S1 at 37 °C for various times. The cleavage reaction was terminated with 3 μL gel loading buffer and analyzed by electrophoresis on a 12% polyacrylamide gel.

NMR measurements

The oligoribonucleotides 5′-GCAAAUCAGUCCG-3′ (13mer) and 5′-GGACAGGGACUUGCG-3′ (15mer), which form a Ni^{2+}-binding RNA motif, were synthesized chemically on a Gene Assembler Plus (Pharmacia) using H-phosphonate synthones (Ott et al., 1994). Purification of the oligonucleotides was performed by HPLC on a Nucleogen-DEAE 500-7 column (Macherey-Nagel).

For NMR measurements, the oligonucleotides (0.17 mM each) were dissolved in 0.5 mL H_2O/D_2O (9:1, v/v) with 100 mM NaCl and 10 mM sodium phosphate, pH 6.5. The sample was annealed by heating to 80 °C for 4 min and slowly cooling to room temperature. Divalent metal ions ($MgCl_2$ and $NiCl_2$ or $MnCl_2$) were added subsequently in small volumes from stock solutions. The NMR spectra were acquired on a DRX 500 spectrometer (Bruker) at a proton resonance frequency of 500 MHz. The 1-3-3-1 pulse sequence (Hore, 1983) was used to suppress the water signal. Chemical shifts were referenced to the methyl resonance of internal DSS (2,2-dimethyl-2-silapentane-5-sulfonate).

UV melting curves

UV melting curves were measured with a spectrophotometer 8452A (Hewlett Packard) equipped with a Peltier element 89090A. The oligoribonucleotides 13mer and 15mer (1.5 μM each) were dissolved in 1 mL of a buffer with 100 mM NaCl, 10 mM sodium phosphate, pH 6.5, and the sample was annealed as described above. $NiCl_2$ or $MgCl_2$ were added subsequently. The absorbance at 260 nm was measured while samples were heated at a rate of 0.5 °C/min.

ACKNOWLEDGMENTS

We thank Dr. M. Yarus for providing DNA for the preparation of randomized RNA. H.-P. H. was a recipient of a scholarship from the Fonds der Chemischen Industrie. This work was supported by the Deutsche Forschungsgemeinschaft, Sp 243/5-2.

Received June 20, 1997; returned for revision August 5, 1997; revised manuscript received August 19, 1997

REFERENCES

Allain FHT, Varani G. 1995. Divalent metal ion binding to a conserved wobble pair defining the upstream site of cleavage of group I self-splicing introns. *Nucleic Acids Res 23*:341–350.

Bartel DP, Zapp ML, Green MR, Szostak JW. 1991. HIV-1 Rev regulation involves recognition of non-Watson–Crick base pairs in viral RNA. *Cell 67*:529–536.

Brown RS, Hingerty BE, Dewan JC, Klug A. 1983. Pb(II)-catalysed cleavage of the sugar–phosphate backbone of yeast $tRNA^{Phe}$: Implications for lead toxicity and self-splicing RNA. *Nature 303*:543–546.

Cate JH, Gooding AR, Podell E, Zhou K, Golden BL, Kundrot CE, Cech TR, Doudna JA. 1996. Crystal structure of a group I ribozyme domain: Principles of RNA packing. *Science 273*:1678–1685.

Christian EL, Yarus M. 1993. Metal coordination sites that contribute to structure and catalysis in the group I intron from *Tetrahymena*. *Biochemistry 32*:4475–4480.

Ciesiolka J, Gorski J, Yarus M. 1995. Selection of an RNA domain that binds Zn^{2+}. *RNA 1*:538–550.

Ciesiolka J, Yarus M. 1996. Small RNA-divalent domains. *RNA 2*:785–793.

Craik DJ, Higgins KA. 1989. NMR studies of ligand–macromolecule interactions. *Annu Rep NMR Spectr 22*:61–138.

Danchin A. 1972. tRNA structure and binding sites for cations. *Biopolymers 11*:1317–1333.

Eichhorn GL, Shin YA. 1968. Interaction of metal ions with polynucleotides and related compounds. XII. The relative effect of various metal ions on DNA helicity. *J Am Chem Soc 90*:7323–7328.

Ellington AD, Szostak JW. 1990. In vitro selection of RNA molecules that bind specific ligands. *Nature 346*:818–822.

Grosshans CA, Cech TR. 1989. Metal ion requirements for sequence-specific endoribonuclease activity of the *Tetrahymena* ribozyme. *Biochemistry 28*:6888–6894.

Hausinger RP. 1993. *Biochemistry of nickel*. New York: Plenum Press.

Hore PJ. 1983. A new method for water suppression in the proton NMR spectra of aqueous solutions. *J Magn Reson 54*:539–542.

Hurd RE, Azhderian E, Reid BR. 1979. Paramagnetic ion effects on the nuclear magnetic resonance spectrum of transfer ribonucleic acid: Assignment of the 15–48 tertiary resonance. *Biochemistry 18*:4012–4017.

Jabri E, Carr MB, Hausinger RP, Karplus PA. 1995. The crystal structure of urease from *Klebsiella aerogenes*. *Science 268*:998–1004.

Jack A, Ladner JE, Rhodes D, Brown RS, Klug A. 1977. A crystallographic study of metal-binding to yeast phenylalanine transfer RNA. *J Mol Biol 111*:315–328.

Jenison RD, Gill SC, Pardi A, Polisky B. 1994. High-resolution molecular discrimination by RNA. *Science 263*:1425–1429.

Kazakov S, Altman S. 1991. Site-specific cleavage by metal ion cofactors and inhibitors of M1 RNA, the catalytic subunit of RNase P from *Escherichia coli*. *Proc Natl Acad Sci USA 88*:9193–9197.

Lehman N, Joyce GF. 1993. Evolution in vitro of an RNA enzyme with altered metal dependence. *Nature 361*:182–185.

Leonard GA, McAuley-Hecht KE, Ebel S, Lough DM, Brown T, Hunter WN. 1994. Crystal and molecular structure of r(CGCG AAUUAGCG): An RNA duplex containing two G(*anti*):A(*anti*) base pairs. *Structure 2*:483–494.

Limmer S. 1997. Mismatch base pairs in RNA. *Prog Nucleic Acid Res Mol Biol 57*. Forthcoming.

Lorsch JR, Szostak JW. 1996. Chance and necessity in the selection of nucleic acid catalysts. *Acc Chem Res 29*:103–110.

Moratel JM, Martinez-Ferrer MJ, Donaire A, Castells J, Salgado J, Jiménez HR. 1991. Spectroscopic studies of nickel(II) carbonic anhydrase and its adducts with inorganic anions. *J Chem Soc Dalton Trans*:3393–3399.

Ott G, Arnold L, Limmer S. 1993. Proton NMR studies of manganese ion binding to tRNA-derived acceptor arm duplexes. *Nucleic Acids Res. 21*:5859–5864.

Ott G, Arnold L, Smrt J, Sobkowski M, Limmer S, Hofmann HP, Sprinzl M. 1994. The chemical synthesis of biochemically active oligoribonucleotides using dimethylaminomethylene protected purine H-phosphonates. *Nucleosides Nucleotides 13*:1069–1085.

Pan T, Long DM, Uhlenbeck OC. 1993. Divalent metal ions in RNA folding and catalysis. In: Gesteland R, Atkins J, eds. *The RNA world*. Cold Spring Harbor, New York: Cold Spring Harbor Laboratory Press. pp 271–302.

Pan T, Uhlenbeck OC. 1992a. A small metalloribozyme with a two-step mechanism. *Nature 358*:560–563.

Pan T, Uhlenbeck OC. 1992b. In vitro selection of RNAs that undergo autolytic cleavage with Pb^{2+}. *Biochemistry 31*:3887–3895.

Pley HW, Flaherty KM, McKay DB. 1994. Three-dimensional structure of a hammerhead ribozyme. *Nature 372*:68–74.

Pyle AM. 1993. Ribozymes: A distinct class of metalloenzymes. *Science 261*:709–714

Rosenthal HE. 1967. A graphic method for the determination and presentation of binding parameters in a complex system. *Anal Biochem 20*:525–532.

Rubin JR, Wang J, Sundaralingam M. 1983. X-ray diffraction study of the zinc(II) binding sites in yeast phenylalanine transfer RNA—Preferential binding of zinc to guanines in purine–purine sequences. *Biochim Biophys Acta 756*:111–118.

Salgado J, Jiménez HR, Moratel JM, Kroes S, Warmerdam GCM, Canters GW. 1996. Paramagnetic cobalt and nickel derivatives of *Alcaligenes denitrificans* azurin and its M121Q mutant. A ^{1}H NMR study. *Biochemistry 35*:1810–1819.

SantaLucia JJ, Kierzek R, Turner DH. 1990. Effects of GA mismatches on the structure and thermodynamics of RNA internal loops. *Biochemistry 29*:8813–8819.

Scatchard G. 1949. Attractions of proteins for small molecules and ions. *Ann NY Acad Sci 51*:660–672.

Schimmel PR, Redfield AG. 1980. Transfer RNA in solutions: Selected topics. *Annu Rev Biophys Bioeng 9*:181–221.

Schreier AA, Schimmel PR. 1974. Interaction of manganese with fragments, complementary fragment recombinations, and whole molecules of yeast phenylalanine specific transfer RNA. *J Mol Biol 86*:601–620.

Scott WG, Finch JT, Klug A. 1995. The crystal structure of an all-RNA hammerhead ribozyme: A proposed mechanism for RNA catalytic cleavage. *Cell 81*:991–1002.

Scott WG, Murray JB, Arnold JRP, Stoddard BL, Klug A. 1996. Capturing the structure of a catalytic RNA intermediate: The hammerhead ribozyme. *Science 274*:2065–2069

Tuerk C, Gold L. 1990. Systematic evolution of ligands by exponential enrichment: RNA ligands to bacteriophage T4 DNA polymerase. *Science 249*:505–510.

Uphoff KW, Bell SD, Ellington AD. 1996. In vitro selection of aptamers: The dearth of pure reason. *Curr Opin Struct Biol 6*:281–288.

Wimberly B. 1994. A common RNA loop motif as a docking module and its function in the hammerhead ribozyme. *Nature Struct Biol 1*:820–827.

Wimberly B, Varani G, Tinoco I Jr. 1993. The conformation of loop E of eukaryotic 5S ribosomal RNA. *Biochemistry 32*:1078–1087.

Wu M, SantaLucia J Jr, Turner DH. 1997. Solution structure of r(GGCAGGCC)$_2$ by two-dimensional NMR and the iterative relaxation matrix approach. *Biochemistry 36*:4449–4460.

Wu M, Turner DH. 1996. Solution structure of (rGCGGACGC)$_2$ by two-dimensional NMR and the iterative relaxation matrix approach. *Biochemistry 35*:9677–9689.

Yarus M. 1993. How many catalytic RNAs? Ions and the Cheshire cat conjecture. *FASEB J 7*:31–39

Zuker M. 1989. On finding all suboptimal foldings of an RNA molecule. *Science 244*:48–52.